Catalysis Science & Technology

Accepted Manuscript

ROYAL SOCIETY OF CHEMISTRY

www.rsc.org/catalysis

Journal Name

RSCPublishing

ARTICLE

Effects of Subnanometer Silver Clusters on Photocatalyst AgBr(110) Surface: A Theoretical Investigation

Cite this: DOI: 10.1039/x0xx00000x

Received 00th XX 2015,
Accepted 00th XX 2015

DOI: 10.1039/x0xx00000x

www.rsc.org/

Yuhua Chi,[a b] Lianming Zhao,[a b] Xiaoqing Lu,[a b] Changhua An,[a b] Wenyue Guo,[*a b] Yunqi Liu,[** c] and Chi-Man Lawrence Wu[d]

The geometrical and electronic structures, and photocatalytic performances of subnanometer clusters Ag_n (n = 2 – 6) deposited on AgBr(110) are studied under the framework of density functional theory (DFT) plus Hubbard U contributions. The most stable adsorption is facilitated by AgBr(110) interacting with the most stable structure of Ag_n and results in a new metal induced gap band (MIGB) located between the valence (VB) and conduction bands (CB). Both the MIGB and CB are mainly contributed by the sp hybridization states from the metal clusters, while the VB comprises primarily the 4p states of surface Br and the 4d states of Ag from both the adsorbate and the surface. The variety of the electronic structures favors the visible and infrared light absorption, which strengthens substantially as the cluster size is enlarged. The dominant localization of the photo-excited electrons on the Ag_n clusters facilitates the oxidation-reduction reactions occurring on the surface and reduces effectively the photolysis of AgBr under the sunlight irradiation. The overpotentials of the CB and VB edges indicate that photocatalytic conversion of CO_2 with H_2O to methanol is possible on AgBr(110) deposited with the Ag_n clusters which has been realized experimentally.

1. Introduction

Nano- and subnano-meter sized metallic clusters deposited on semiconductor supports are of great interest because of their importance in heterogeneous catalysis.[1-5] For the subnanometer metal clusters consisting of several atoms, it has been shown that strong metal-support interaction can directly affect the dispersion of the metal clusters as well as the adsorption geometries and electronic structures of the materials, and as a result enhances their catalytic activity towards reactions such as CO oxidation,[6,7] photocatalytic degradation of organic compounds[8] and water-gas shift (WGS),[9] etc.

The catalytic properties of semiconductors have been found to vary with the geometry as well as the size of the deposited subnanometer clusters. Lei et al. found that alumina supported Ag_3 clusters and ~3.5 nanometer Ag nanoparticles can catalyze the direct propylene epoxidation with high activity at low temperatures.[10] Lee et al. studied the Au_n/TiO_2 (n = 1 – 7) catalysts and found that the CO oxidation activity varied strongly with the deposited cluster sizes, with a significant activity appearing at Au_3.[11] Kaden et al. explored the CO reaction with O_2 catalyzed by Pd_n/TiO_2 (n=1, 2, 4, 7, 10, 16, 20, 25) using temperature programmed reaction (TPR) mass spectrometry and X-ray photoemission spectroscopy (XPS), and found Pd_{20} had exceptionally high efficiency for molecular oxygen activation.[12] Li et al. studied the size- and shape-dependent catalytic activities of Au_n/TiO_2 (n =1 – 4, 7, 16 – 20) by means of density functional theory (DFT) calculations and microkinetics analysis, and found the catalytic activities increased with the size n up to Au_{18}, and the hollow-cage Au_{18} isomer exhibited the highest activity for CO oxidation.[13]

The effects of metal clusters on support surfaces can be described by two aspects. On one hand, the clusters can potentially introduce gap states into the band gap of the semiconductors.[14,15] On the other hand, the clusters can serve as a co-catalyst to reduce the recombination of e^-/h^+ pairs and also as plasmonic particles to increase the concentration of the photoexcited electrons.[16,17] Clarifying the effects of the deposited metal clusters needs a deep and systematic understanding of the geometrical, electronic and optical properties of the cluster-support adsorption systems.

Recently, silver halides, plasmonic photocatalysts, have become a hot topic in photocatalysis because of their strong visible light absorption and photosensitive characteristics.[18-22] These materials are expected to have important applications in the energy and environmental fields, but are seldom used as photocatalysts due to their instability under sunlight. Fortunately, Kakuta et al. found that AgBr decomposition to Ag occurred in the early stages of UV illumination, but covered with Ag clusters it was stable under successive UV illumination.[23] Inspired by this finding, this material has attracted wide attention and has been extensively studied to explore the light absorption properties and photocatalytic performances. Studies concerning the behavior of silver halides supported Ag clusters suggested that Ag/AgBr nanoplates

exhibited stronger visible-light absorption and higher stability than pristine AgBr, due to the fact that photons are only absorbed by the silver nanoparticles.[24,25] Kuai et al. prepared Ag/AgBr by a facile hydrothermal and subsequently sun-light-induced formation method, and found that the as-prepared AgBr covered with Ag clusters had a strong absorption in the visible region, which was almost as strong as that in the UV region due to the plasmon resonance of the silver nanoparticles deposited on AgBr. This material was stable due to the fact that photons were only absorbed by the silver nanoparticles and electrons separated by the absorbed photons remained in the nanoparticles rather than being transferred to the Ag^+ ions of the AgBr lattice.[26] Xu et al. prepared plasmonic photocatalyst Ag/AgBr with a facile method in ionic liquid, and found silver halides could maintain stability if the Ag clusters were well dispersed on the silver halide; this material displayed high photocatalytic activity towards the methyl orange (MO) dye degradation, which increased as the Ag/AgBr nanoparticles size was reduced and could be attributed to the presence of Ag clusters.[27]

Indeed, depositing Ag clusters on silver bromide has been extensively found to enhance the photocatalytic activity under the visible light irradiation, not only towards degradation of organic pollutants but also towards conversion of CO_2 to methanol. The influence of the silver clusters was explained by using surface plasmon resonance (SPR) produced by the collective oscillations of surface electrons.[28,29] However, theoretical study of the photocatalytic properties of silver bromide supported silver clusters is rarely reported, even though it is very important for understanding their stabilities and photocatalytic performances.

Very recently, we studied the optical and photocatalytic properties of the atomic Ag adsorbed AgBr(110) and AgBr(100) surfaces based on periodic slab model and DFT.[30] Our results show that the adsorption of atomic Ag modifies the electronic structures of the AgBr surfaces, that is, a metal induced gap band (MIGB) is formed between the valence band (VB) and conduction band (CB) and the CB comprises primarily the s/p states of the adsorbates, which enhances the visible and infrared light absorption coefficients. Also, among all the surfaces studied, the atomic Ag adsorbed (110) surface was found to have the highest photocatalytic activity for H_2O dissociation. In this work, we extend our study to AgBr(110) supported subnanometer clusters Ag_n (n = 2 – 6) using DFT. The purpose of this work is to clarify how subnanometer silver clusters affect the electronic structures, optical properties and photocatalytic performances of AgBr.

2. Methods and Computational Details

The calculations were performed based on DFT with the Perdew-Burke-Ernzerhof (PBE) form of the general gradient approximation (GGA) functional. A plane wave basis set and norm-conserving pseudopotentials were used as implemented in the CASTEP program.[31-33] The basis plane waves limited to a maximum cutoff energy of 450 eV were utilized to expand valence electrons. The slabs were separated by a vacuum region of 15 Å, which is large enough to prevent the artificial interaction between the distinct slabs. The valence configurations were $4d^{10}5s^1$ for Ag and $4s^24p^5$ for Br. The parameters setting in the calculations were as follows: the force on atoms was less than 0.03 eV/Å, the stress on atoms was less than 0.05 GPa, the atomic displacement was less than 0.001 Å, and the energy variation was less than 1×10^{-5} eV/atom. In order to describe properly the band gaps and the positions of additional states introduced by adsorbed metal clusters, the LDA+U formalism was incorporated in the DFT calculations, the U value was chosen as $U_{d,Ag}$ = 1.6 eV, $U_{p,Br}$ = 1.3 eV.[30]

The initial stable structures of the Ag_n clusters were calculated firstly by using the $Dmol^3$ programs within the general gradient approximation PBE (GGA-PBE) and DNP basis set and then calculated with CASTEP using the parameters as mentioned above. The stable adsorption configurations of Ag_n/AgBr(110) were optimized using CASTEP, with the assumed initial configurations by placing the most stable Ag_n clusters on the AgBr(110) surface. The substrate contained six atomic layers with the 12.24 Å thickness. The relevant adsorbates Ag_n and the uppermost two atomic layers of the slab were allowed to relax, while the other atoms were fixed at their bulk positions. The present calculation indicated that the surface energy changes slightly (by 0.0036 J/m^2) when the thickness increases from four (0.0948 J/m^2) to six (0.0984J/m^2) atomic layers. Therefore, the selected six-layer slab was satisfactory to describe the features of the AgBr surface.

The binding energy was computed by using the following formula:

$$E_b = \left(E_{Ag_n} - nE_{Ag}\right)/n$$

where E_{Ag_n} is the total energy of the Ag_n cluster, E_{Ag} is the total energy of the Ag atom, n is the number of Ag atoms.

The Ag_n-AgBr interaction was described by the adsorption energy, E_{ads}, defined as[4]

$$E_{ads} = (nE_{Ag} + E_{AgBr} - E_{Ag_n/AgBr})/n$$

where E_{AgBr} and $E_{Ag_n/AgBr}$ are the total energies of the clean AgBr slab and the Ag_n/AgBr adsorption system, respectively. By this definition, a positive value of the adsorption energy means a stable adsorption.

The (2 × 2) supercell was adopted in this study. Because the larger supercell can release the strain energy associated with the adsorption of the silver clusters, the adsorption energies of Ag_n/AgBr(110) calculated using the (3 × 3) supercell were found to be higher than those from the (2 × 2) supercell. However, these two models predicted a same rule, i.e., odd-even oscillations, for the adsorption energies (see Fig. S1, in the Electronic Supplementary Information (ESI)). The odd-even oscillations can be contributed to the Ag cluster properties as a function of the number of the metal atoms.[34]

The absorption coefficients of the materials were calculated using the following relation[35,36]

$$\alpha(\omega) = \sqrt{2}\omega[\sqrt{\varepsilon_1(\omega)^2 + \varepsilon_2(\omega)^2} - \varepsilon_1(\omega)]^{1/2}$$

where $\varepsilon_1(\omega)$ and $\varepsilon_2(\omega)$ are the real and imaginary parts of the dielectric tensor of the materials, respectively.

3. Results and discussion

3.1 Geometrical structures

The structure of the clean AgBr(110) surface has been reported by us very recently.[30] Generally, the surface has a saw-tooth stepped structure, in which the step edges are formed with four-coordinate silver and bromine atoms alternatively along the [001] direction, and the saw-tooth trough along $[1\bar{1}0]$ is constructed alternatively by the V-type Ag-Br-Ag and Br-Ag-Br groups, as shown in Fig. 1a.

3.1.1. Free Ag_n clusters. A variety of possible initial structures of the free silver clusters Ag_n (n = 2 – 6) are optimized, and the most stable structures are shown in Fig. 1. Fig. S2, in the ESI, give the second most stable structures for

comparison. For Ag_2, the calculated bond length of 2.61 Å is close to the experimental (2.535 Å[37]) and theoretical (2.6112 Å[38]) values. For the other clusters considered, planar structures are preferred. The structure of Ag_3 is an equilateral triangle with the side of 2.68 Å (see Fig. 1c). Ag_4 has a rhombus structure (see Fig. 1d), in which the four rhombus sides are 2.78 Å long and the shorter diagonal length is 2.67 Å. The Ag_5 structure is an isosceles trapezium (see Fig. 1e), in which the upper and lower bases are constructed by two and three Ag atoms with the bond lengths of 2.84 and 2.74 Å, respectively, and the legs are 2.77 Å. Ag_6 forms also an equilateral trianglar structure, with the side and inside bonds of 2.74 and 2.85 Å long (see Fig. 1f). We can find that the bonds in the most stable structures are shorter than those in the corresponding second most stable structures. As the Ag_n size is growing, the binding energy of the clusters decreases slightly for the first two and then increases monotonously for the others (see Fig. 1). These calculated results are in agreement with the results reported in references.[38,39]

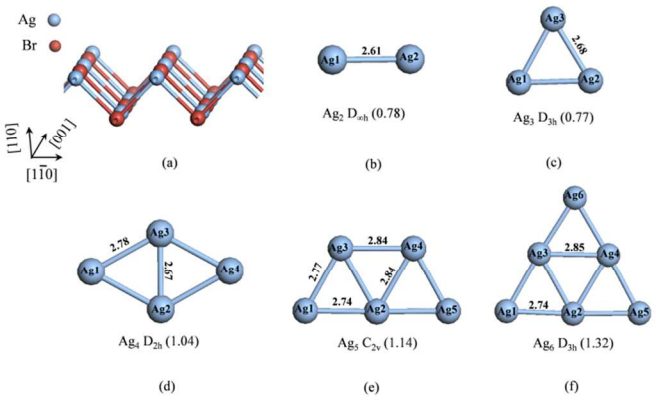

Fig. 1. The structures of clean AgBr(110) surface and the most stable state of free clusters Ag_n (n = 2 - 6) with the bond lengths in Å. Given below are the symmetry groups and the binding energies in eV.

3.1.2. Ag_n/AgBr(110) adsorption systems. Multiple possible initial adsorption configurations of Ag_n on AgBr(110), such as vertical, horizontal and inclined adsorptions (see Fig. S3), are optimized. The most stable structures are shown in Fig. 2. The lengths of the newly-formed bonds are given in Table 1. For comparison, the second and third most stable structures are given in Fig. S4, in the ESI, and the adsorption energies are given in Fig. S5, in the ESI. For the most stable adsorption of Ag_2/AgBr(110) (see Fig. 2a), the Ag_2 dimer crosses the plane of an Ag-Br-Ag group and bridges the V edges, favoring an nearly parallel location with the tilt angle of 8.9°, in which $Ag1_{ad}$ and $Ag2_{ad}$ shares the two edge Ag atoms in the Ag-Br-Ag group. In addition, $Ag1_{ad}$ binds also to all atoms in adjacent Br-Ag-Br group, and $Ag2_{ad}$ attaches to one more edge Br atom from the other adjacent Br-Ag-Br group. The adsorption results in remarkable stretching of the Ag_2 bond (2.83 vs. 2.61 Å).

The triangular Ag_3 is upright adsorbed on AgBr(110) via $Ag1_{ad}$ and $Ag2_{ad}$. $Ag3_{ad}$ bridges $Ag1_{ad}$-$Ag2_{ad}$ at the distance of 2.82 Å, largely stretched from that in the free trimer (2.68 Å) (Fig. 2b). The interaction of $Ag1_{ad}$-$Ag2_{ad}$ with surface is quite similar to the Ag_2 adsorption, but in this case it takes to a larger extent the parallel fashion so that $Ag2_{ad}$ attaches directly to two edge Br atoms. The average lengths of the cluster-edge Ag-Ag and Ag-Br bonds are 2.91 and 2.85 Å, longer than those in Ag_2/AgBr(110) (2.86 and 2.83 Å).

For tetramer Ag_4 (Fig. 2c), the adsorption of the planar rhombus is analogous to the trimer adsorption via one out of the four rhombus sides ($Ag1_{ad}$-$Ag2_{ad}$), with the fourth $Ag4_{ad}$ bridging $Ag2_{ad}$-$Ag3_{ad}$ at the distances of 2.90 and 2.76 Å. The obvious difference is that $Ag1_{ad}$ is only bound directly to one edge Br, i.e., $Br2_{ed}$. The average lengths of the cluster-edge Ag-Ag and Ag-Br bonds (2.89 and 2.84 Å) are longer than those in Ag_2/AgBr(110), but are shorter than those in Ag_3/AgBr(110).

The planar Ag_5 is also upright adsorbed on AgBr(110), along the [001] direction (see Fig. 2d). However, the interaction in this case is quite different from those of Ag_n/AgBr(110) (n = 2 – 4), i.e., through two Ag atoms (center and corner) on the longer base side of the trapezium, in which the center $Ag2_{ad}$ is located above an Ag-Br-Ag group and bridges the two edge Ag atoms, and the corner $Ag1_{ad}$ interacts with adjacent Br-Ag-Br group. This adsorption predicts a large tilt to the surface for the longer base side as well as a large variation in the surface structure, that is, the relevant edge Ag-Br bonds are broken and correspondingly the Ag-Ag bond is strengthened.

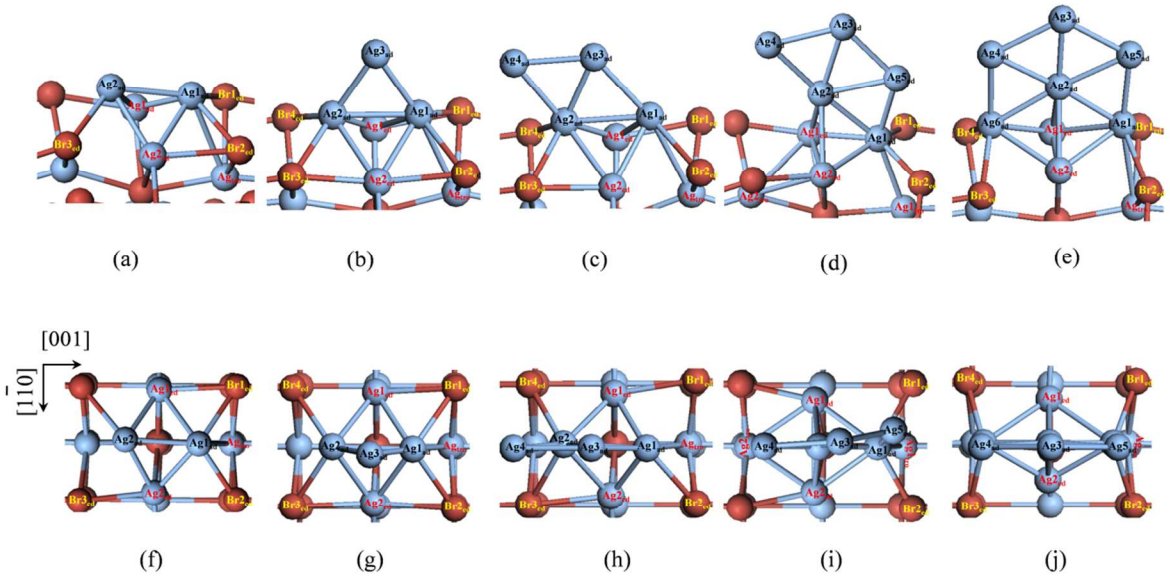

Fig. 2. The most stable structures of Ag_n/AgBr(110). Silver and bromine atoms are indicated as light blue and wine spheres. Side and top views of (a) and (f) Ag_2/AgBr(110), (b) and (g) Ag_3/AgBr(110), (c) and (h) Ag_4/AgBr(110), (d) and (i) Ag_5/AgBr(110) and (e) and (j) Ag_6/AgBr(110).

Table 1. Bond lengths (Å) for Ag_n adsorbed on the AgBr(110) surface.

Bonds	Ag_2	Ag_3	Ag_4	Ag_5	Ag_6
$Ag1_{ad}/Ag6_{ad}$-$Ag1_{ed}$	2.848	2.909	2.855	2.826	3.011/2.910
$Ag1_{ad}/Ag6_{ad}$-$Ag2_{ed}$	2.860	2.898	2.850	2.826	2.895/3.069
$Ag1_{ad}$-Ag_{tro}	3.308	3.274	3.357	3.055	3.337
$Ag2_{ad}$-$Ag1_{ed}$	2.866	2.898	2.915	2.956	3.083
$Ag2_{ad}$-$Ag2_{ed}$	2.864	2.918	2.940	2.954	2.944
$Ag1_{ad}$-$Br1_{ed}$	2.784	2.856		2.655	2.781
$Ag1_{ad}$-$Br2_{ed}$	2.827	2.860	2.882	2.688	2.718
$Ag2_{ad}/Ag6_{ad}$-$Br3_{ed}$	2.880	2.877	2.822		2.727
$Ag2_{ad}/Ag6_{ad}$-$Br4_{ed}$		2.803	2.831		2.823

The adsorption of Ag_6 is more complicated (Fig. 2e). Although the most stable structure of free Ag_6 is an equilateral triangle, the most stable adsorption leads to a configuration that the adsorbate changes to a fan-shaped structure with one atom at the center and five atoms on the edge. The triangular Ag_6 adsorption is the 3rd most stable state of Ag_6/AgBr(110) (see Fig. S4i, in the ESI). The adsorption of the fan-shaped cluster is quite analogous to the situation of Ag_5, with the sixth metal atom ($Ag6_{ad}$) binding directly to the two edge Br atoms from the other adjacent Br-Ag-Br group (see Fig. 2e). The average bond lengths of $Ag1_{ad}$ and $Ag6_{ad}$ with the two edge Ag atoms are 2.95 and 2.98 Å, and those with the edge Br atoms are 2.75 and 2.77 Å, both of which are close to each other, suggesting the cluster is nearly symmetrically adsorbed on the surface.

Similar to the situation of Au_n/TiO_2,[4] the adsorption energies of Ag_n/AgBr(110) shown in Fig. S1, in the ESI, exhibit a weak odd-even oscillation rule, i.e., up for the even-number clusters and down for the odd-number clusters.

3.2 Electronic structures

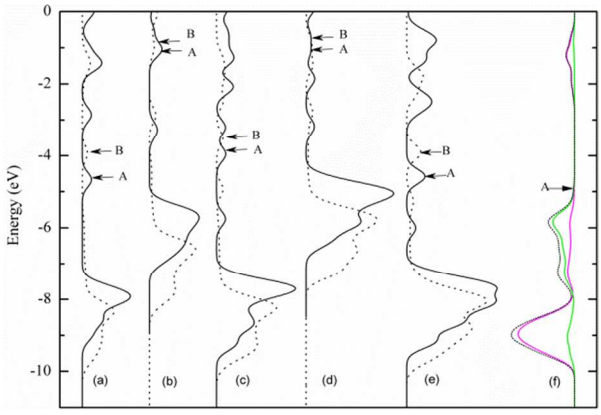

Fig. 3. Total density of states (TDOS) of free and adsorbed Ag_n clusters as well as the clean AgBr(110) surface. Black solid and dot lines are for the free and adsorbed states, short dot line is for the AgBr surface, magenta and green lines are for surface Ag and Br atoms, respectively. The energy is referred to the vacuum level. A and B denote the Fermi level of the free and adsorbed systems. (a) Ag_2, (b) Ag_3, (c) Ag_4, (d) Ag_5, (e) Ag_6 and (f) clean surface.

The DOSs of the clean and atomic Ag adsorbed AgBr(110) have been investigated recently.[30] Generally, the DOS of the clean AgBr(110) shows a strong VB in the range of -4.9 – 0.3 eV and a weak CB in the region of 2.5 – 4.5 eV, with the band gap of 2.2 eV. The VB comprises dominant Ag 4d and Br 4p and minor Ag 5s and Ag 5p, and near the maximum (VBM) dominantly contributed is Br 4p; the CB is contributed by the Ag 5s and 5p states. After the adsorption of atomic Ag, the VB of AgBr(110) changes slightly, but the CB splits into two bands, i.e., the MIGB (from -0.5 to 0.9 eV) arising from the bonding interaction of the 5s and 5p states of Ag_{ad} and Ag_{ed}, and the CB (from 1.4 to 2.9 eV) consisting of the antibonding interaction of the relevant states of Ag_{ad} and Ag_{ed} (mainly Ag_{ad} 5p and Ag_{ed} 5s).

3.2.1 Free Ag_n clusters. The total density of states (TDOSs) of the free Ag_n clusters is shown in Fig. 3. The TDOSs of the adsorbed Ag_n clusters, the TDOSs and atomic partial density of states (PDOSs) of the free AgBr(110) surface are also given for comparison. The vacuum energy level is selected as the energetic zero. For all the free Ag_n, there is a strong and broad band, contributed mainly by the Ag d states, located in the lowest energy region of interest. Above the band, there are several weak bands due to the sp hybridizations of Ag. The sp molecular orbitals of the Ag_n clusters are shown in Fig. S6, in the ESI. It is interesting to note that the Fermi level as well as the bands of the odd number Ag_n clusters is higher in energy than those of the clusters with even-number atoms, agreeing with the odd-even oscillation phenomena of the ionization potentials, electron affinities and vertical detachment energies of Ag_n clusters reported previously.[34,39] The adsorption of Ag_n on AgBr(110) results in the broadening as well as the downward going of the d band, especially in the case of the odd-number Ag_n clusters, following the order of $\Delta d_{n=3} > \Delta d_{n=5} > \Delta d_{n=4} > \Delta d_{n=2} > \Delta d_{n=6}$ (see Table S1, in the ESI). Meanwhile, the sp hybridized states go upwards, resulting in the slight uprights of the Fermi level. This may be due to the increase of p-state components in the sp mixing states, as shown in Fig. S7, in the ESI.

3.2.2 Ag_n/AgBr(110) adsorption systems. The PDOSs of the most stable adsorption configurations of Ag_n/AgBr(110) are examined. Fig. 4 shows the PDOSs of the relevant atoms in the energy region of interest. For comparison, the sum of the local DOSs of all Ag and Br atoms in the first layer of the adsorbed surface is also given. The energy zero corresponds to the Fermi level of the respective adsorption system. Fig. S8, in the ESI, shows the isosurface plots of the electronic wave functions of the considered bands of Ag_n/AgBr(110) together with those of the VBM and CBM of the clean AgBr(110). Similar to the atomic Ag adsorption,[30] the adsorption of Ag_n clusters leads always to three separated bands, located below, across and above the Fermi level in most cases. The Ag_3 adsorption is an exception, which gives a different position of the bands, i.e., two below and one across the Fermi level, as a result of the high location of the Fermi level of free Ag_3 (see Fig. 3). Analogous to the situation of the Ag/AgBr(110) system,[30] these bands correspond to the VB, MIGB and CB.

The VB is located in the region of -7.8 – -2.4 eV for Ag_3/AgBr(110) and about -6.5 – -1.1 eV for others. This band is contributed primarily by the states of the atoms involved in the cluster-surface interaction, i.e., the Ag_{ad} 4d, Ag_{ed} 4d and Br_{ed} 4p states, showing strong and considerable mixing of Ag_{ad} 4d with Ag_{ed} 4d and Br_{ed} 4p, respectively. In addition, contribution of the Ag_{tro} 4d states is also significant (see Fig. S9, in the ESI). The situation near the VBM, however, is more complex, because of the possibility of mixing with the upper states. For Ag_2/AgBr(110) and Ag_3/AgBr(110), similar to the

situation of AgBr(110) and Ag/AgBr(110),[30] only the Br_{ed} 4p states contribute largely to the VBM, while the VBM of the larger Ag_n/AgBr(110) (n = 4 – 6) systems also comprises largely the lowest sp hybridized state of the Ag atoms binding directly to the surface (Fig. 4 and Fig. S8, in the ESI).

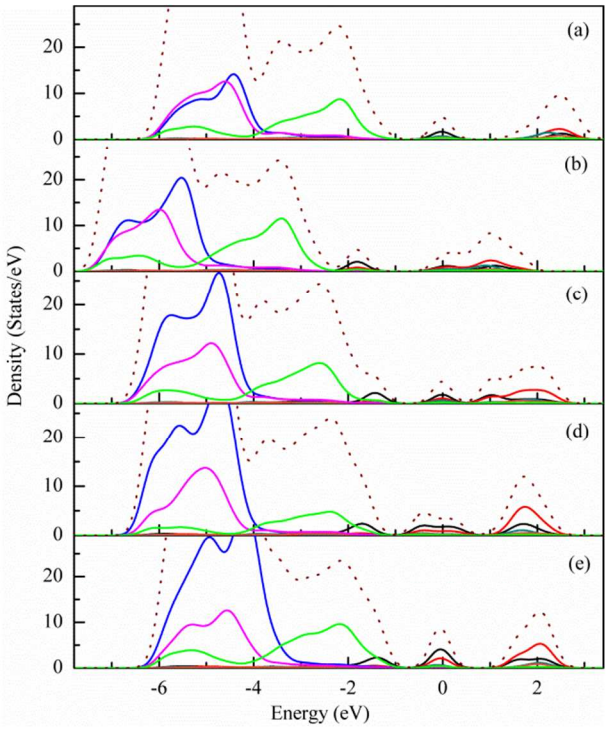

Fig. 4. Partial density of states (PDOSs) of cluster Ag 5s, 5p, 4d, surface Ag 5s, 5p, 4d and Br 4p states for (a) Ag_2/AgBr(110), (b) Ag_3/AgBr(110), (c) Ag_4/AgBr(110), (d) Ag_5/AgBr(110), (e) Ag_6/AgBr(110). Black line is for Ag_{ad} 5s, red line is for Ag_{ad} 5p, blue line is for Ag_{ad} 4d, dark cyan line is for Ag_{ed} 5s, orange line is for Ag_{ed} 5p, magenta line is for Ag_{ed} 4d, green line is for Br_{ed} 4p, and wine dot line is the sum of the local DOS of all Ag and Br atoms in the first layer of the adsorbed system. The energy is referenced to the Fermi level of the Ag_n/AgBr system.

The MIGB is centered at about -1.8 eV for Ag_3/AgBr(110) and close to the Fermi level for others. The band is contributed by the lowest sp hybridized (bonding) state for the Ag_2 and Ag_3 adsorption (see Fig. S8, in the ESI) and the second lowest sp hybridized state for the Ag_4 and Ag_6 adsorption. The Ag_5 adsorption predicts a broad and bimodal DOS (-0.93 – 0.69 eV) for the MIGB, which is formed by the overlap of two bands, as mirrored by the molecular orbitals (see Fig. S8, in the ESI). In all cases, the corresponding orbitals of the MIGB are mainly localized in the metal clusters (see Fig. S8, in the ESI), and the relative contribution follows Ag_{ad} 5s > Ag_{ad} 5p > Ag_{ed} 5s. The gap of the band to the VB for the odd-number clusters (0.1 – 0.2 eV) is narrower than that of the clusters with even-number metal atoms (0.3 – 0.5 eV).

The CB of Ag_3/AgBr(110) is found to cross the Fermi level, while for the others it is located above the Fermi level. The wide and bimodal DOS features indicate that it is overlapped by two bands for n = 3, 4 and 6, whereas for the others only one band is involved. This band is located above the MIGB with a narrow gap for Ag_4 (0.1 eV) and relatively wide gaps for the others (0.5 – 0.7 eV). In all cases, the corresponding orbitals of the CB are also mainly localized in the metal clusters (see Fig. S8, in the ESI), and the relative contribution follows Ag_{ad} 5p > Ag_{ad} 5s > Ag_{ed} 5s > Ag_{ed} 5p. For comparison, the PDOSs of the second most stable structures are given in Fig. S10, in the ESI, and the main features similar to those of the most stable structures are found in the figures.

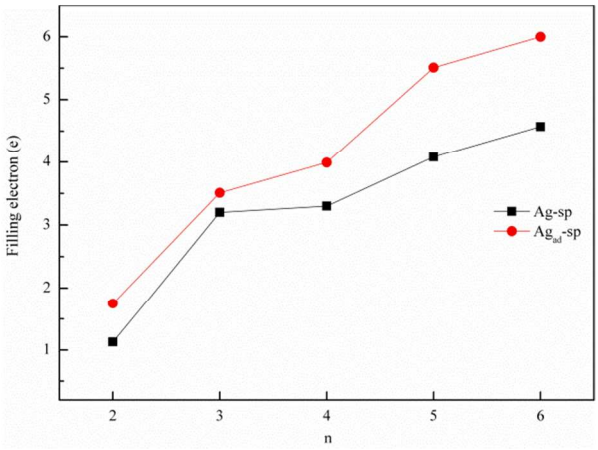

Fig. 5. The sp filling electrons of the Ag_n clusters in free (black line) and adsorbed (red line) states.

We also calculated the charges in the Ag_n clusters by integrating the PDOS of the relevant states from the lowest energy level of interest to the Fermi level. In consistent with the higher location of the Fermi level of the silver clusters compared to the clean AgBr surface (see Fig. 3), the adsorption results in slight transfer of electrons from the Ag_n clusters to the AgBr surface, mirrored by the decrease of electrons on adsorbed silver clusters by about 0.31 – 0.52 e (see Fig. S11a, in the ESI). The electrons lost from the silver clusters are found to primarily come from the d orbitals, while the sp electrons indeed increase by 0.31 – 1.43 e (see Fig. 5). The increase of the sp electrons is expected to facilitate the catalytic reactions occurring on the surface because the relevant states are near the Fermi level.[30] Furthermore, the electrons in the sp states show an increase trend with the growth of the Ag_n clusters (Fig. 5), indicating an enhancement of the surface plasmon of metal clusters on the surface

3.3 Optical properties

Fig. 6 presents the absorption spectra of the Ag_n/AgBr(110) (n = 2 – 6) systems. Different from the situation that pure AgBr only shows the UV absorption,[26] absorptions of the Ag_n adsorption systems are extensive in the UV, visible and infrared regions. Except for Ag_3/AgBr(110), the absorption spectra of Ag_n/AgBr(110) show obviously the bimodal features, i.e., a sharp peak in the UV region corresponding to the fundamental absorption of the pure AgBr(110) surface,[30] and a wide peak in the visible region arising from the Ag_n adsorption, in good agreement with the experimental spectra reported in references.[27,40,41] The growth of Ag_n clusters changes slightly the position of the UV peak, but results obviously in the red-shift of the visible peak. Meanwhile, the change of the cluster size largely suppresses the optical absorption in the UV region and remarkably enhances the absorption in the visible and infrared region so that the UV and visible absorption peaks are indeed comparable (35584 and 26065cm^{-1}, respectively) for the largest system of Ag_6/AgBr(110). The Ag_3 adsorption system, however, presents the strongest UV and largely frustrated visible absorptions so that the visible absorption peak is not observed but instead a long tail extended from the UV peak is

present. The absorption spectra of the second most stable structures are also studied (see Fig. S12, in the ESI). Although there are slight differences in the UV region, similar characters to that of the most stable structures are shown, especially in the visible region. Thus, if the structures of Ag_n/AgBr(110) applied are not the most stable ones, the main conclusions in this study are not changed.

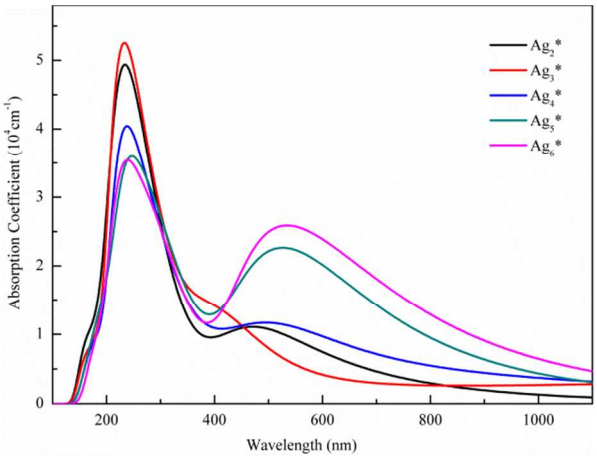

Fig. 6. The calculated optical absorption coefficients for the Ag_n/AgBr(110) surfaces.

Based on the DOSs and electronic wave functions as shown in Fig. 4 and Fig. S8, in the ESI, the fundamental UV absorption excites the VB to CB transition, attributed mainly to the photo-excitation of electrons from the surface Br 4p states to the 5s/5p states of the Ag_n clusters. In the final state, the main contribution of the Ag_{ad} 5p states rather than the Ag_{ed} 5s state as for atomic Ag adsorbed AgBr(110)[30] reduces the intrinsic photo-excitation of electrons from Br to Ag in AgBr (Br 4p → Ag 5s) and thus enhances the stability of the material. The visible absorption is attributed to the MIGB to CB transition, resulting mainly in the photo-induced electron transfers between different electronic states of the adsorbed clusters. The much close location of the MIGB to the VB for Ag_3/AgBr(110) indicates that the absorption spectrum arising from these two bands would overlap with each other and thus shows a strong UV peak together with a long tail in the red side as shown in Fig. 6. The infrared absorption arises from the VB maximum to MIGB transition, i.e., Br 4p → Ag_{ad} 5s/5p, as well as the MIGB to CB transition, i.e., the Ag 5s bonding state to the Ag 5p antibonding states.

It is clear that under the irradiation of sunlight the photo-excited electrons in the Ag_n adsorbed AgBr(110) systems would transfer dominantly to the adsorbed Ag_n clusters, facilitating the reduction of organic species occurring on these metal atoms as well as oxidation reactions on Br atoms. This result explains the surface plasmon resonance of metal nanoparticles on the catalyst surfaces under visible light.[24, 25]

3.4 Photocatalytic performances

In addition to the excellent photocatalytic activity to degrade MO dye and rhodamine-B,[21, 22] the Ag/AgBr nanocomposites also showed high catalytic activity on conversion of CO_2 with H_2O to energetic fuels, e.g., methanol/ethanol, under visible light irradiation, through **Reaction 1**,[28]

$$CO_2 + 2H_2O \rightarrow CH_3OH + 3/2O_2 \qquad (\mathbf{1})$$

Reaction 1 contains two half reactions as follows,

$$CO_2 + 6H^+ + 6e^- \rightarrow CH_3OH + H_2O \qquad (\mathbf{1'})$$

$$H_2O \rightarrow 1/2O_2 + 2H^+ + 2e^- \qquad (\mathbf{1''})$$

For **Reactions 1′** and **1″**, the electrode potentials $\varphi^{\Theta}(CO_2/CH_3OH)$ and $\varphi^{\Theta}(H_2O/H^+)$ are -0.38 and 0.815 eV (vs NHE), respectively. If the whole photocatalytic reation (**Reaction 1**) is possible, the edge of the CB (E_{CB}) of the photocatalysts should be more negative than $\varphi^{\Theta}(CO_2/CH_3OH)$, enabling the photogenerated electrons on the photocatalysts to convert CO_2 to CH_3OH through **Reaction 1′**, and also the edge of the VB (E_{VB}) should be more positive than $\varphi^{\Theta}(H_2O/H^+)$, rendering the photogenerated holes over the photocatalysts to oxidize water to generate hydrogen ions via the other half reaction of **Reaction 1″.**

The CB and VB edges of Ag_n/AgBr(110) can be calculated, respectively, by using equation $E_{CB} = X - E_C - 0.5E_g$ and $E_{VB} = E_g + E_{CB}$,[28] where X is the electronegativity of the semiconductors, E_C represents the energy of free electrons on the hydrogen scale (4.5 eV), and E_g represents the band gap of the systems, which can be estimated from the calculated absorption spectra (see Fig. S13, in the ESI).

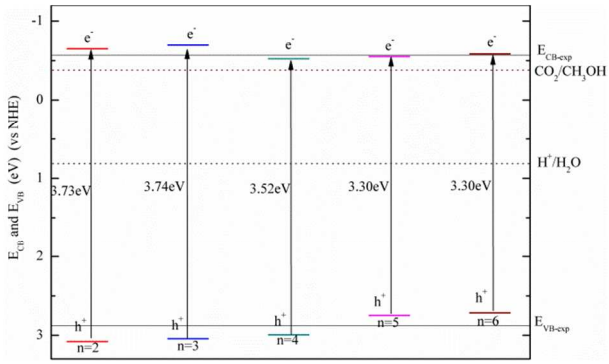

Fig. 7. The positions of E_{CB} and E_{VB} of Ag_n/AgBr(110). Solid and dot lines represent the experimental values of E_{CB} and E_{VB} of Ag/AgBr nanoplates and the potentials $\varphi^{\Theta}(CO_2/CH_3OH)$ and $\varphi^{\Theta}(H_2O/H^+)$, respectively.

Fig. 7 shows the positions of E_{CB} and E_{VB} for the Ag_n/AgBr(110) (n = 2 – 6) surfaces with the experimental values[28] of Ag/AgBr nanoplates. The overpotentials are at least 1.9 and 0.15 eV for E_{VB} and E_{CB} of the systems, suggesting that the photogenerated electrons and holes can react with adsorbed CO_2 and H_2O to produce methanol. Clearly, the Ag_n/AgBr catalysts have much strong oxidation abilities and relatively weak reduction abilities, which is agreement with the experimental result. The oxidation ability show a monotonous decrease trend as the cluster size is enlarged, but the obvious change takes place at n = 4 to 5, showing nearly comparable higher and lower oxidation abilities than the experimental results for the smaller (n = 2 – 4) and larger (n = 5 and 6) clusters deposited, respectively. The variety of the reduction ability is relatively smooth. When the cluster is enlarged, the reduction ability of the first two clusters increases slightly so as to reach the highest one at n = 3, then abruptly decreases at n = 3 to 4, and finally increases for the last larger clusters gradually closing to the experimental values. Moreover, the energy gap decreases as the cluster is growing, favoring the longer-wavelength light absorption, as shown in Fig. 6.

The adsorption of CO_2 as the first step of the photocatalytic conversion is very important for photocatalytic CO_2 conversion

with water. To deeply understand the photocatalytic surface processes, the adsorption properties of CO_2 on the Ag_n/AgBr(110) (n = 2 - 6) surfaces were further calculated. The computational details are shown in Section S1, in the ESI.

The calculated results suggest that some reconstruction of the Ag_n cluster occurs during CO_2 adsorption on the substrate surfaces (see Fig.S14, in the ESI), which is due to the fluxionality characteristic of the subnanometer metal cluster. A similar situation is also found in the CO_2 adsorption on the $Ag_8(Pt_8)/TiO_2(101)$ surface.[42] The C−O bond length of adsorbed CO_2 is about 0.01 - 0.02 Å longer than that of free CO_2 molecule (1.082 Å), suggesting that the adsorbed CO_2 molecule is activated by the metal center (see Fig.S14, in the ESI). The adsorption energy of CO_2 on the Ag_n/AgBr(110) (n = 2 - 6) surfaces are shown in Fig. 8. With the increase of the Ag cluster size, the adsorption energy increases from 0.226 eV for n =2 to 0.299 ev for n=3, then obviously decreases to 0.183 eV at n=4, and finally increases for the Ag_n (n = 5, 6) clusters (0.276 and 0.345 eV). The results are in good agreement with the reduction ability as discussed above.

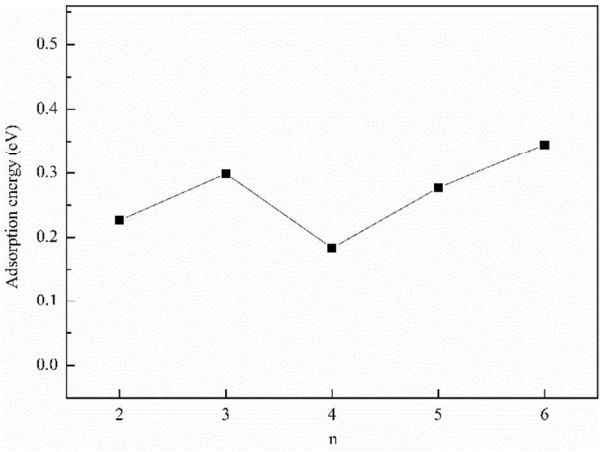

Fig. 8. The adsorption energy of CO_2 on the Ag_n/AgBr(110) (n = 2-6) surfaces.

In summary, the smaller Ag_n clusters (n = 2 and especially 3) deposited on the AgBr(110) surface favor the both the oxidation and reduction reactions in the conversion of CO_2 with H_2O to methanol, but disfavor the visible and infrared light absorption. In the case of the larger clusters, especially Ag_6 deposited, in spite of the slight expense of the oxidation and reduction abilities, the substantial strengthening of the visible and infrared light absorption is expected to improve sunlight-utilization ratio for the conversion of CO_2 with H_2O to methanol.

4. Conclusions

In this article, we have systematically investigated the geometrical and electronic structures, light absorption properties and photocatalytic performances of Ag_n/AgBr(110) (n = 2 – 6) using the framework of DFT plus Hubbard U contributions. The main conclusions are as follows.

Among the possible structures of the Ag_n clusters, the planar structures are always preferred in the free and adsorption states. The adsorption of Ag_n on AgBr(110) shows weak odd-even oscillations in adsorption energies and induces a new MIGB located between the VB and CB. Both the MIGB and CB are mainly contributed by the s/p states from the metal clusters, while the VB comprises primarily the surface Br 4p states and the 4d states of Ag from both the adsorbate and the surface. The position and composition of these bands are tuned by the number of the metal atoms in the clusters. The variety of the electronic structures of AgBr(110) induced by the Ag_n clusters favors the visible and infrared light absorption, which strengthens substantially as the cluster size is enlarged, and thus improves the sunlight utilization. The exception is for Ag_3/AgBr(110), in which the absorption spectrum shows an strong UV peak together with a long tail in the visible region. The dominant localization of the photo-excited electrons on the Ag_n clusters facilitates the oxidation-reduction reactions occurring on the surface and also reduces effectively the photolysis of AgBr under the sunlight irradiation. The overpotentials of the CB and VB edges indicate that photocatalytic conversion of CO_2 with H_2O to methanol is possible on AgBr(110) deposited with the Ag_n clusters, and deposition of the smallest two clusters is the most favorable for both the relevant oxidation and reduction reactions. However, in spite of slight expense of the oxidation and reduction abilities, the substantial strengthening of the visible and infrared light absorption is expected to improve sunlight-utilization ratio for the conversion of CO_2 with H_2O into methanol on the AgBr(110) surface deposited with the larger clusters (especially Ag_6).

Acknowledgements

This work was supported by the Program for NSFC (21303266), Promotive Research Fund for Excellent Young and Middle-aged Scientists of Shandong Province (BS2012NJ015), and the Fundamental Research Funds for the Central Universities (14CX02004A, 14CX06001A, 13CX02001A, 13CX05020A and 15CX08010A).

Notes and references

[a] *College of Science, China University of Petroleum, Qingdao, Shandong 266580, P. R. China*
[b] *Key Laboratory of New Energy Physics & Materials Science in Universities of Shandong Province, China University of Petroleum, Qingdao, Shandong 266580, P. R. China*
[c] *State Key Laboratory of Heavy Oil Processing, Key Laboratory of Catalysis, CNPC, China University of Petroleum, Qingdao 266580, P. R. China*
[d] *Department of Physics and Materials Science, City University of Hong Kong, Hong Kong SAR, P. R. China*
E-mail: wyguo@upc.edu.cn (W. Guo); liuyq@upc.edu.cn (Y. Liu).

† Electronic Supplementary Information (ESI) available: The second most stable structures of silver cluster Ag_n (n = 3 – 6), and the structure parameters; The adsorption mode for Ag_n on AgBr(110) surface; The isosurface plots of the free clusters; The PDOS of Ag_{tro}; The second and third most stable structures, the isosurface plots of electronic wave function and the band gap estimation for Ag_n/AgBr(110) (n = 2 – 6) surfaces. The PDOS and the absorption spectra of the second most stable structures of adsorption systems. The adsorption structures of CO_2 on Ag_n/AgBr(110) (n = 2 – 6) and the computational details. See DOI: 10.1039/b000000x/

1 S. J. Tauster, S. C. Fung, R. T. K. Baker and J. A. Horsley, *Science* **1981**, 211, 1121.
2 M. A. Vannice and B. Sen, *J. Catal.* **1989**, 115, 65.
3 S. Gilb, P. Weis, F. Furche, R. Ahlrichs and M. M. Kappes, *J. Chem. Phys.* **2002**, 116, 4094.
4 C.H. Sun and S. C. Smith, *J. Phys. Chem. C* **2012**, 116, 3524.
5 C. T. Yang, N. Balakrishnan, V. R. Bhethanabotla and B. Joseph, *J. Phys. Chem. C* **2014**, 118, 4702.

6 W. E. Kaden, T. P. Wu, W. A. Kunkel and S. L. Anderson, *Science* **2009**, 326, 826.
7 B. Yoon, H. Häkkinen, U. Landman, A. S. Wörz, J.-M. Antonietti, S. Abbet, K. Judai and U. Heiz, *Science* **2005**, 307, 403.
8 S. Hong and T. S. Rahman, *J. Am. Chem. Soc.* **2013**, 135, 7629.
9 J. A. Rodríguez, J. Evans, J. Graciani, J.-B. Park, P. Liu, J. Hrbek and J. F. Sanz, *J. Phys. Chem. C* **2009**, 113, 7364.
10 Y. Lei, F. Mehmood, S. Lee, J. Greeley, B. Lee, S. Seifert, R. E. Winans, J. W. Elam, R. J. Meyer, P. C. Redfern, D. Teschner, R. Schlögl, M. J. Pellin, L. A. Curtiss and S. Vajda, *Science* **2010**, 328, 224.
11 S. Lee, C. Fan, T. Wu and S. L. Anderson, *J. Chem. Phys.* **2005**, 123, 124710.
12 W. E. Kaden, W. A. Kunkel, M. D. Kane, F. S. Roberts and S. L. Anderson, *J. Am. Chem. Soc.* **2010**, 132 (38), 13097.
13 L. Li, Y. Gao, H. Li, Y. Zhao, Y. Pei, Z. F. Chen and X. C. Zeng, *J. Am. Chem. Soc.* **2013**, 135, 19336.
14 Y. Han, C. j. Liu and Q. Ge, *J. Phys. Chem. B* **2006**, 110, 7463.
15 G. Stephan, C. Gion and H. Roald, *Chem. Eur. J.* **2002**, 8, 1785.
16 S. Linic, P. Christopher and D. B. Ingram, *Nat. Mater.* **2011**, 10, 911.
17 W. Hou, W. H. Hung, P. Pavaskar, A. Goeppert, M. Aykol and S. B. Cronin, *ACS Catal.* **2011**, 1, 929.
18 M. R. Elahifard, S. Rahimnejad, S. Haghighi and M. R. Gholami, *J. Am. Chem. Soc.* **2007**, 129, 9552-9553.
19 L. S. Zhang, K. H. Wong, H. Y. Yip, C. Hu, J. C. Yu, C. Y. Chan and P. K. Wong, *Environ. Sci. Technol.* **2010**, 44, 1392.
20 H. F. Cheng, B. B. Huang, P. Wang, Z. Y. Wang, Z. Z. Lou, J. P. Wang, X. Y. Qin, X. Y. Zhang and Y. Dai, *Chem. Commun.* **2011**, 47, 7054.
21 H. Wang, J. Yang, X. Li, H. Zhang, J. Li and L. Guo, *Small* **2012**, 8, 1.
22 H. Wang, X. Lang, J. Gao, W. Liu, D. Wu, Y. Wu, L. Guo and J. Li, *Chem. Eur. J.* **2012**, 18, 4620.
23 N. Kakuta, N. Goto, H. Ohwaki and T. Mizushima, *J. Phys. Chem. B* **1999**, 103, 5917.
24 P. Wang, B. B. Huang, X. Y. Zhang, X. Y. Qin, Y. Dai, H. Jin, J. Y. Wei and M. H. Whangbo, *Chem. Eur. J.* **2009**, 15, 1821.
25 C. Hu, Y. Q. Lan, J. H. Qu, X. X. Hu and A. M. Wang, *J. Phys. Chem. B* **2006**, 110, 4066.
26 L. Kuai, B. Geng, X. Chen, Y. Zhao and Y. Luo, *Langmuir* **2010**, 26, 18723.
27 H. Xu, Y. Song, L. Liu, H. Li, Y. Xu, J. Xia, X. Wu and S. Zhao, *J. Chem. Technol. Biotechnol.* **2012**, 87, 1626.
28 C. An, J. Wang, W. Jiang, M. Zhang, X. Ming, S. Wang and Q. Zhang, *Nanoscale* **2012**, 4, 5646.
29 C. An, J. Wang, C. Qin, W. Jiang, S. Wang, Y. Li and Q. Zhang, *J. Mater. Chem.* **2012**, 22, 13153.
30 Y. H. Chi, L. M. Zhao, X. Q. Lu and W. Y. Guo, *RSC Adv.* **2014**, 4, 33134.
31 P. E. Blöchl, *Phys. Rev. B* **1994**, 50, 17953.
32 G. Kresse and J. Joubert, J. *Phys. Rev. B* **1999**, 59, 1758.
33 J. P. Perdew, K. Burke and M. Ernzerhof, *Phys. Rev. Lett.* **1996**, 77, 3865.
34 R. Fourniera, *J. Chem. Phys.* **2001**, 115, 2165.
35 B. Modak, K. Srinivasu and S. K. Ghosh, *J. Phys. Chem. C* **2014**, 118, 10711.
36 J. Sun and H.T. Wang, *Phys. Rev. B* **2005**, 71, 125132.
37 V. Beutel, H. G. Kramer and G. L. Bhale, *J. Chem. Phys.* **1993**, 98, 2699.
38 X. B. Li, H. Wang, Y. Tang, G. Xu, H. Mao, C. Li and Z. Zhu, *J. At. Mol. Phys.* **2004**, 21, 388.
39 B. K. Vlasta, V. Vincent and M. Roland, *J. Chem. Phys.* **2001**, 115, 10450.
40 P. Wang, B. B. Huang, X. Y. Qin, X. Y. Zhang, Y. Dai, Z. Wang and Z. Lou, *ChemCatChem* **2011**, 3, 360.
41 L. Nie, Z. Huang, H. Xu, W. Zhang, B. Yang, L. Fang and S. Li, *Chin. J. Catal.* **2012**, 33, 1209.
42 C.-T. Yang, B. C. Wood, V. R. Bhethanabotla, and B. Joseph, *J. Phys. Chem. C* **2014**, 118, 26236.